Distinct Subpopulations of Nucleus Accumbens Dynorphin Neurons Drive Aversion and Reward

Highlights

- Optogenetic excitation of nucleus accumbens dynorphin cells elicits dynorphin release

- Discrete accumbens shell dynorphinergic populations drive either aversion or reward

- These two nucleus accumbens subregions can be bi-directionally controlled

- Both aversive and rewarding behaviors require kappa opioid receptors

Authors

Ream Al-Hasani, Jordan G. McCall, Gunchul Shin, ..., Thomas L. Kash, John A. Rogers, Michael R. Bruchas

Correspondence

alhasanir@morpheus.wustl.edu (R.A.-H.), bruchasm@wustl.edu (M.R.B.)

In Brief

Al-Hasani et al. show that dynorphin is necessary to drive opposing motivational states within subregions of the nucleus accumbens shell. Dynorphinergic neurons in the ventral shell drive aversion whereas in the dorsal shell they drive preference and reward seeking.

Distinct Subpopulations of Nucleus Accumbens Dynorphin Neurons Drive Aversion and Reward

Ream Al-Hasani,[1],[10],[*] Jordan G. McCall,[1],[9],[10] Gunchul Shin,[2] Adrian M. Gomez,[1] Gavin P. Schmitz,[1] Julio M. Bernardi,[3] Chang-O. Pyo,[4] Sung Il Park,[2] Catherine M. Marcinkiewcz,[5] Nicole A. Crowley,[5] Michael J. Krashes,[6],[7],[8] Bradford B. Lowell,[8] Thomas L. Kash,[5] John A. Rogers,[2],[4] and Michael R. Bruchas[1],[9],[*]

[1]Departments of Anesthesiology, Division of Basic Research, Anatomy and Neurobiology, Division of Biomedical Engineering and Washington University Pain Center, Washington University School of Medicine, Saint Louis, MO 63110, USA
[2]Department of Materials Science and Engineering, Frederick Seitz Materials Research Laboratory, University of Illinois at Urbana-Champaign, Urbana, IL 61801, USA
[3]Department of Psychiatry, Washington University School of Medicine, Saint Louis, MO 63110, USA
[4]Department of Electrical and Computer Engineering, Frederick Seitz Materials Research Laboratory, University of Illinois at Urbana-Champaign, Urbana, IL 61801, USA
[5]Department of Pharmacology and Bowles Center for Alcohol Studies, School of Medicine, University of North Carolina, Chapel Hill, Chapel Hill, NC 27516, USA
[6]Diabetes, Endocrinology and Obesity Branch, National Institute of Diabetes and Digestive and Kidney Diseases, National Institutes of Health, Bethesda, MD 20892, USA
[7]National Institute on Drug Abuse, National Institutes of Health, Baltimore, MD 21224, USA
[8]Division of Endocrinology, Department of Medicine, Beth Israel Deaconess Medical Center, Harvard Medical School, Boston, MA 02115, USA
[9]Division of Biology and Biomedical Sciences, Washington University School of Medicine, Saint Louis, MO 63110, USA
[10]Co-first author
*Correspondence: alhasanir@morpheus.wustl.edu (R.A.-H.), bruchasm@wustl.edu (M.R.B.)
http://dx.doi.org/10.1016/j.neuron.2015.08.019

SUMMARY

The nucleus accumbens (NAc) and the dynorphinergic system are widely implicated in motivated behaviors. Prior studies have shown that activation of the dynorphin-kappa opioid receptor (KOR) system leads to aversive, dysphoria-like behavior. However, the endogenous sources of dynorphin in these circuits remain unknown. We investigated whether dynorphinergic neuronal firing in the NAc is sufficient to induce aversive behaviors. We found that photostimulation of dynorphinergic cells in the ventral NAc shell elicits robust conditioned and real-time aversive behavior via KOR activation, and in contrast, photostimulation of dorsal NAc shell dynorphin cells induced a KOR-mediated place preference and was positively reinforcing. These results show previously unknown discrete subregions of dynorphin-containing cells in the NAc shell that selectively drive opposing behaviors. Understanding the discrete regional specificity by which NAc dynorphinerigic cells regulate preference and aversion provides insight into motivated behaviors that are dysregulated in stress, reward, and psychiatric disease.

INTRODUCTION

It is now widely thought that many mood disorders are associated with major disruption of the brain's reward circuitry. The nucleus accumbens (NAc) is a key region in this circuit with major projections from the ventral tegmental area (VTA), medial prefrontal cortex (mPFC), basolateral amygdala (BLA), and hippocampus (Britt et al., 2012; Russo and Nestler, 2013). Recent studies have identified the striatum as crucial for integrating behavioral responses to both positive and negative reinforcement (Castro and Berridge, 2014; Everitt and Robbins, 2005; Kravitz et al., 2012). For example, NAc neuronal activity is consistently reduced in major depression in humans (Drevets et al., 1992; Mayberg et al., 2000) and is thought to reflect a loss of reward function that drives common symptoms such as anhedonia (Russo and Nestler, 2013). In order to better understand these processes, it is important to dissect how neuromodulator systems within specific brain subnuclei function to influence negative emotional states, represented by changes in motivated behavior.

The kappa opioid receptor (KOR) system has been identified as one such prominent neuromodulator system in the regulation of motivated behavior and is highly implicated in stress-induced dysphoria and vulnerability to drug abuse. KORs are endogenously activated by the peptide dynorphin (dyn), which is cleaved from the precursor prodynorphin (Chavkin et al., 1982). Dyn is widely known to mediate negative emotional states; for example, KOR agonists induce place aversions, depression-like behavior, and dysphoria in both human and animal models (Mucha et al., 1985; Pfeiffer et al., 1986; Shippenberg et al., 2007). Notably, direct infusion of KOR agonists into the NAc mediates conditioned place aversion (Bals-Kubik et al., 1989), and local antagonism of KOR in this region prevents depression-like behavioral responses (Land et al., 2009; Shirayama et al., 2004). Furthermore, dyn-containing axon terminals and cell bodies are located in the NAc (Van Bockstaele et al.,
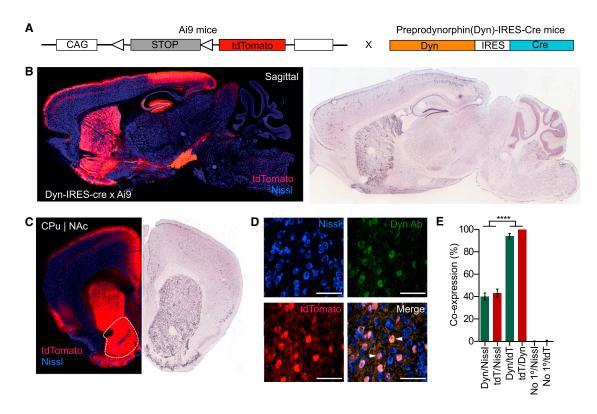
Figure 1. Dyn-tdTomato-Reporter Mouse Allows Visualization of Dynorphin-Containing Cells

(A) Diagram showing the generation of the dyn-Cre^tdTomato mouse line from the cross between the dyn-IRES-cre x Ai9-tdTomato.

(B) Dyn labeling in dyn-IRES-cre x Ai9-tdTomato compared to in situ images from the Allen Institute for Brain Science in a sagittal section highlighting presence of dyn in the striatum, the hippocampus, BNST, amygdala, hippocampus, and substantia nigra. All images show tdTomato (red) and Nissl (blue) staining.

(C) Coronal section highlighting dynorphinergic cell labeling in the NAc as compared to the Allen Institute for Brain Science.

(D) Images of nissl (blue), tdtomato (red), and dyn (green) and a merge of all three in the NAcSh (63× magnification) (AP+1.3, ML ±0.5, DV−4.5). All scale bars are 100 μm.

(E) Cells labeled with anti-dyn antisera also all express tdtomato represented as co-expression (%). This is significant when compared to dyn/nissl co-localization (data represented as mean ± SEM, n = 3 slices per animal from three animals per group: one way ANOVA, Bonferroni post hoc, dyn/nissl versus dyn/tdtomato, dyn/nissl versus no1°/Nissl, tdTomato/Nissl td/Tomato/dyn, and tdTomato/Dyn versus no1°/tdtomato, ****p < 0.0001).

1995), and a number of studies have shown recruitment of the dyn/KOR system within the NAc following compulsive drug taking (Daunais et al., 1993; Fagergren et al., 2003; Hurd et al., 1992; Lindholm et al., 2000; Schlussman et al., 2005; Solecki et al., 2009). It is thought that monoamine output within the NAc is tightly regulated via presynaptic KORs on serotonergic and dopaminergic cells in the region, ultimately acting to suppress release of dopamine and serotonin. However, the mechanisms and role of endogenous dyn in the regulation of KOR-mediated negative affective behaviors remain unresolved (Bruchas et al., 2010, 2011).

Here we directly ascertained the sufficiency of the photostimulation of dyn-expressing cells within the NAc shell (NAcSh) to drive motivated behaviors. We hypothesized that photostimulation of dyn-expressing cells the NAcSh will drive an aversion behavior in a real-time place-testing paradigm (RTPT) using a combination of bidirectional wireless μ-ILED optogenetic technology, a conditioned place-testing paradigm and operant self-stimulation. Here we report a distinct subpopulation of ventral NAc dyn-expressing cells that when photostimulated produce robust aversive behavioral responses, whereas photostimulation

of dyn-expressing cells in a nearby dorsal NAc site engages positively reinforced motivated behaviors, both of which of require KOR activation.

RESULTS

Dyn-tdTomato-Reporter Mouse Allows Visualization of Dynorphin-Containing Cells

To determine key sites of dyn influence throughout the brain, we generated a dyn-tdTomato-reporter mouse by crossing preprodynorphin-IRES-cre (dyn-IRES-cre) mice (Krashes et al., 2014) to the Allen Institute for Brain Science tdTomato flox-stop reporter line (Ai9) (Madisen et al., 2010) (Figures 1A and S1). This new mouse line (dyn-cre^tdTomato) is useful for cre-dependent expression/excision in selected dyn-circuits and provides a representative map of dyn-expressing cells, dyn axon projections, and terminal fields. We first characterized dyn expression across the full brain of these mice, comparing our dyn-cre^tdTomato expression with in situ hybridization data (Figures 1B and 1C) to confirm soma-specific labeling in well-known dyn-enriched regions. Using dyn-cre^tdTomato mice, we visualized an abundance

of dyn-containing cells within the NAc, in line with current literature (Figures 1B and 1C). In addition, we found robust dyn-induced tdTomato expression in the hippocampus, bed nucleus of the stria terminalis, BLA, central nucleus of the amygdala, throughout the cortex, caudate putamen, globus pallidus, VTA and the substania nigra, dorsal raphe, and locus coeruleus (Figures S1A–S1E).

To further validate our reporter mouse, we first examined whether both dyn- and tdTomato-labeled cells are expressed in the same number of nissl-labeled cells within the NAcSh. In these experiments, we found that 100% of cells labeled with the anti-dyn antisera also express tdTomato (Figures 1D, 1E, and S1F). This was statistically significant and highly conserved, as not all dyn-labeled cells overlaid with all the nissl-labeled cells. We also ran a negative control in which the primary antibody was absent, further confirming the integrity of the anti-dyn antisera (Figures 1E and S1F). These findings support the conclusion that the dyn-cre^{tdTomato} mouse line reliably labels dyn-containing cells in the NAc.

Photostimulation of Dyn-Containing Cells Elicits Action Potential Firing and Release of Dynorphin
Due to the relative novelty of this dyn-cre mouse line, we first determined whether photostimulation of dyn-containing cells could elicit robust action potentials at multiple frequencies in slice. We injected AAV5-DIO-ChR2-eYFP into the NAc of dyn-cre mice (Figure 2A) and performed whole-cell electrophysiology. We found intact spike fidelity at frequencies of 5 Hz, 10 Hz, and 20 Hz (1 ms, 5 ms, and 10 ms pulse width), which was not stably maintained at 40 Hz (Figures 2B–2F, S2A, and S2B). Importantly, we also demonstrate that when we pulse blue light on cells that express ChR2, we see reliable spiking in current clamp; however, when we pulse blue light on cells that do not express ChR2 in close proximity, we see no effects in current clamp, supporting the notion that interactions between dyn-positive cells and neighboring medium spiny neurons (MSNs) or cholinergic neurons are not observed under these photostimulation conditions. We then performed several experiments in voltage clamp in non-ChR2-expressing neurons and found evidence for local GABA release onto these non-ChR2 neurons, consistent with models that suggest different populations of MSNs can inhibit each other (Figure S2C).

To ascertain whether photostimulation of these cells could lead to dyn release at a frequency of 10 Hz (10 ms pulse width), we established an optogenetically induced neuropeptide release ELISA in tissue slice. Here we show that photostimulation of ChR2-expressing neurons in the NAcSh of dyn-cre mice significantly increases the release of dyn compared to non-ChR2-expressing neurons in controls (dyn-cre$^-$ mice) (Figures 2G, 2H, and S2D). Taken together, these data support the conclusion that we can reliably drive dynorphinergic tone in dyn-expressing cells in the NAc.

Activation of Dynorphinergic Cells in the NAcSh Drives Both Aversion and Reward
Prior reports have suggested that the dyn/KOR system mediates negative emotional states associated with depression and drug dependence through increased dyn expression and release in

the NAc, contributing to the dysphoria. However, the endogenous source of dyn in these responses has not been shown (Britton et al., 1982; Bruchas et al., 2010; Knoll et al., 2011; Lindholm et al., 2000; Mucha et al., 1985; Pfeiffer et al., 1986; Rylkova et al., 2009; Schlosburg et al., 2013; Shippenberg et al., 2007). Given the location of dyn-expressing cells in the NAc, we first hypothesized that photostimulation of NAc-dyn neurons would produce aversive behaviors. To test this hypothesis, we injected AAV5-DIO-ChR2-eYFP, chronically implanted a fiber optic into the NAcSh of dyn-cre$^+$ and dyn-cre$^-$ mice (controls), and used an RTPT (Figure 3A). During this 20-min behavioral test, photostimulation occurs in real-time only upon entry into the counterbalanced designated chamber (Carter et al., 2010; Siuda et al., 2015a; Stamatakis and Stuber, 2012; Tan et al., 2012). Behavioral data were then calculated as time spent in the photostimulation-paired chamber, expressed as a percentage of total time. In this experiment we also assessed the efficacy of photostimulated cell firing in vivo in producing real-time behavioral responses, as compared to the in vitro whole-cell recordings. In accordance with our hypothesis, we found that photostimulation of dyn-expressing cells in the NAcSh over the same range of frequencies (5 Hz, 10 Hz and 20 Hz with an 10 ms pulse width) produced a significant real-time aversion behavior, which plateaued at 40 Hz, correlating with the in vitro whole-cell recordings (Figure 3B). Interestingly we also observed a subgroup of mice that showed a robust preference behavior when compared to controls. To further validate this apparent divergence in behavior, we performed a D'agostino and Pearson Omnibus normality test, which established that these data are not normally distributed (p < 0.001) and are bimodal. This allowed us to further classify the data into two separable groups. To investigate what may drive these opposing behavioral states, we carefully examined the anatomical distribution of viral expression within the NAcSh of each individual mouse and group. Interestingly, we identified that mice exhibiting a preference behavior showed isolated dorsal viral expression in the NAcSh, whereas mice exhibiting an aversion behavior showed a more ventral pattern of viral expression (Figures 3C and S3A). Using a Spearman rank correlation test, we show that the level of preference/aversion (expressed as percent time in stimulation side) in each individual mouse is positively correlated (r = 0.8895) with the location of both viral expression and fiber optic placement along the dorsal-ventral axis (Figures 3D and S3B). Here we report that photostimulation of dyn-expressing cells at −4.60 mm to −5.00 mm from bregma drives an aversion behavior whereas photostimulation of dyn-expressing cells at −4.00 mm to −4.30 mm drives a preference behavior. We therefore classified these two groups as "averters" or "preferers."

Following the identification of two distinct and opposing groups, we analyzed the efficacy of photostimulation frequency to drive these behaviors. We found that both 10 Hz and 20 Hz stimulation produced a real-time place preference in mice with more dorsal viral expression and fiber optic placement, and in contrast, this stimulation pattern elicited an aversion in mice with ventral viral expression and fiber optic placement. These were significantly different from one another and both were significantly different when compared to dyn-cre$^-$ controls injected with AAV5-DIO-ChR2-eYFP (Figures 3E and 3F). These
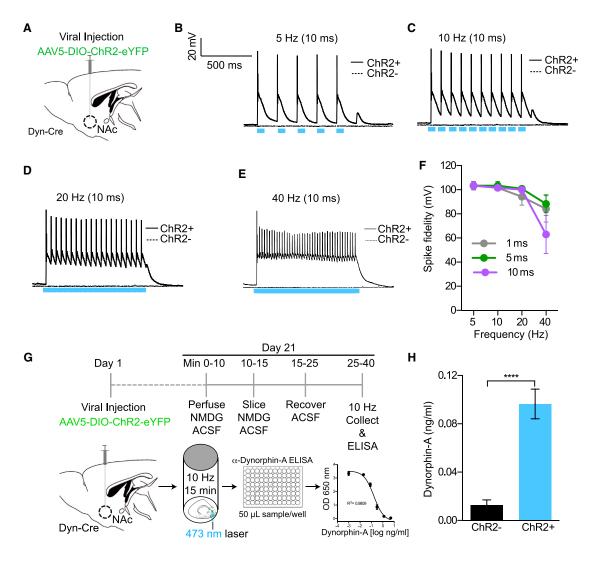
Figure 2. Photostimulation of Dyn-Containing Cells Elicits Action Potential Firing and Release of Dynorphin

(A) Cartoon of virus and fiber optic placement.

(B–E) Whole-cell slice recording showing light-evoked action potentials in dyn-cre ChR2+ and ChR2− cells in the vNAcSh using a 10-ms pulse width at 5, 10, 20, and 40 Hz.
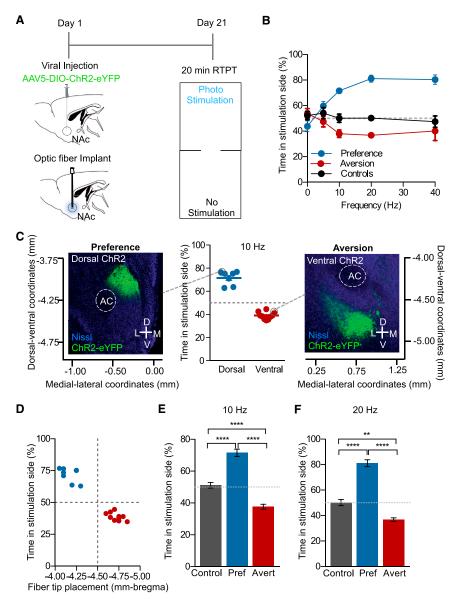
(F) Summary graph showing loss of spike fidelity at 40 Hz and no apparent change in spike fidelity at 1, 5, or 10 ms pulse width.

(G) Timeline used to collect samples and measure dyn release using an ELISA protocol. ACSF = artificial cerebrospinal fluid. NMDG = N-methyl-D-glucamine.

(H) Photostimulation of dyn-expressing ChR2+ cells in the NAcSh increases the concentration of dyn when compared to non-ChR2-expressing cells in dyn-cre− animals (data represented as mean ± SEM, n = 2/group with eight replicates in each group: Student's t test ****p < 0.0001).

results suggest that photostimulation of dyn-expressing cells in discrete subregions within the NAcSh can drive opposing behaviors with distinct positive (dorsal) or negative (ventral) valence as measured by a real-time place preference or real-time place aversion, respectively.

Spatially Discrete Targeting of NAc Dyn-Containing Cells Can Engage Either Preference or Aversion in the Same Animal

To further investigate the subregional distinction in behavior within the NAcSh and to enable precise, discrete spatial targeting, we used a new modified form of our recently developed wireless μ-ILED devices (Jeong et al., 2015; Kim et al., 2013; McCall et al., 2013). We reconfigured the original wireless μ-ILED devices to produce a device that allows isolated and directionally controlled light to specific NAc subregions. In this case, we positioned one μ-ILED to target the dorsal NAcSh (dNAcSh) and the other the ventral NAcSh (vNAcSh), separated by a distance of 1 mm (Figures 4A, 4B, S4A, and S4B). These devices are wirelessly controlled using a radio frequency (RF) power source, which can either activate each μ-ILED independently or both simultaneously (Figures 4B and S4B). These devices provide discrete spatial targeting and importantly allow for selective regional photostimulation within the same individual mouse. Following injection of AAV5-DIO-ChR2-eYFP into the NAcSh of dyn-cre+ and dyn-cre− mice, with expression spanning both

Figure 3. Activation of Dynorphinergic Cells in the NAcSh Drives Both Aversion and Reward

(A) Calendar outlining experimental procedure of the RTPT.

(B) Frequency response curve (10, 20, and 40 Hz stimulation; 10 ms pulse width) showing two distinctly responding groups. One group spent significantly more time in the photostimulation side (preference), and the other spent more time in the non-stimulated side aversion (data represented as mean ± SEM, n = 7–10).

(C) Scatter plot of individual mice that exhibit a preference behavior, show dorsal ChR2 expression, or an aversion behavior, show more ventral ChR2 expression, following 10 Hz, 10 ms pulse width photostimulation (n = 7–10). Nissl (blue) and ChR2 (green).

(D) Scatter plot showing the level of preference in each individual mouse is positively correlated with fiber tip placement (data represented as mean ± SEM, n = 7–10: Spearman positive correlation, r = 0.8895).

(E) At 10 Hz preferers and averters show a significant preference or aversion compared to each another and controls (data represented as mean ± SEM, n = 5–11: one-way ANOVA, Bonferroni post hoc, control versus preferers ****p < 0.0001, control versus averters ****p < 0.01, preferers versus averters ****p < 0.0001).

(F) At 20 Hz preferers and averters show a significant preference or aversion compared to one another and controls (data represented as mean ± SEM, n = 6: one-way ANOVA, Bonferroni post hoc, control versus preferers ****p < 0.0001, control versus averters **p < 0.001, preferers versus averters ****p < 0.0001).

dorsal and ventral coordinates, devices were implanted into mice and used in the real-time place preference paradigm (Figure 4C). Here we show that within the same mouse we can selectively photostimulate the ventral NAc, to produce a real time aversion; photostimulate the dNAcSh, to drive a real time preference; or both regions together, which does not elicit either behavior (Figures 4D–4F). In addition, photostimulation of dyn-expressing cells in either the dorsal or the vNAcSh does not induce any significant changes in locomotor activity compared to controls (Figure S4E). In addition, we investigated whether targeting these distinct regions in the NAc induced anxiety behavior, as recent reports have implicated the KOR/dyn system in anxiety-like behavioral responses (Bruchas et al., 2009; Knoll et al., 2011). Consistent with prior reports that identified the BLA and the central nucleus of the amygdala as key KOR-expressing regions involved in anxiety-like behaviors, we found that stimulating

dyn-containing cells in either dorsal or ventral NAcSh did not induce anxiety-like behavior in an open field anxiety-like behavioral paradigm (Figures S4F–S4I).

Together, these data support the hypothesis that activation of dyn-expressing cells in the vNAcSh drives an aversion behavior and cells in the dNAcSh drives a preference. Bidirectional μ-ILED control adds confidence to the current findings and suggests that stimulation of the subsets of neurons within the NAc dynorphinergic system is capable of dynamic engagement of either positive or negative valence in the same mouse. Furthermore, because these devices are ultrathin, minimally invasive (Jeong et al., 2015; Kim et al., 2013; McCall et al., 2013), and target both dorsal and ventral NAcSh, there is limited likelihood that dorsal lesions from our earlier fiber optic implantation influence the observed behavioral responses.

Dynorphin mRNA-Positive Neurons Colocalize with Drd1-Positive Neurons, but Not with Drd2-Positive Neurons in Both the dNAcSh and vNAcSh

To understand how different populations of dyn-expressing cells with the dorsal or vNAcSh are able to drive opposing behaviors,
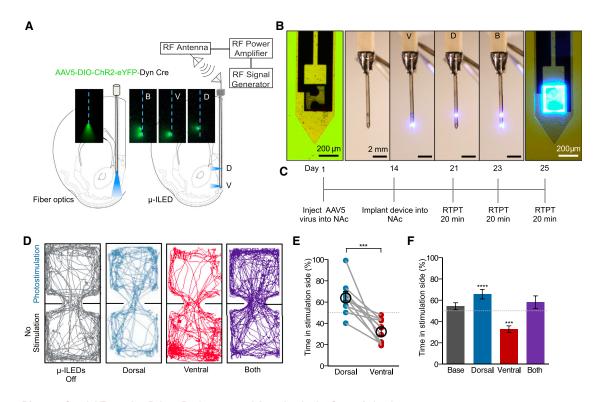
Figure 4. Discrete Spatial Targeting Drives Preference and Aversion in the Same Animal

(A) Directionally controlled light spread of μ-ILED devices compared to fiber optics for isolating subregions of NAc as demonstrated in the fluorescein.

(B) Images of an ultrathin (∼10–50 μm), flexible integrated system. Light can be isolated to either dorsal or ventral NAcSh

(C) Behavioral calendar of the experimental procedure.

(D) Examples of real-time mouse behavioral traces following no stimulation, ventral or dorsal wireless photostimulation, and ventral and dorsal photostimulation together.

(E) Aversion and preference real-time behavior following stimulation of the ventral and dNAcSh within each individual mouse (data represented as mean ± SEM, n = 11: Student's t test, ***p < 0.001).

(F) Stimulation with dorsal μ-ILED drives a real-time place preference, but stimulation with ventral μ-ILED drives an aversion, measured as a significant increase or decrease in time spent in the stimulation side (%), respectively. Stimulating both ventral and dorsal μ-ILEDs has no significant effect on behavior. (Data represented as mean ± SEM, n = 11: one sampled Student's t test; ****p < 0.0001 dorsal and ***p < 0.001 ventral.)

we explored the colocalization of dyn with known dopaminergic receptors using mRNA in situ hybridization. It is widely known that dyn is locally expressed in MSNs within the NAc that coexpress dopamine D1 receptors (Ghazarossian et al., 1980; Raynor et al., 1994), but the discrete regions within the NAcSh identified here have not been extensively examined in this respect. We hypothesized that dopamine D1/Dyn co-expression may differ between the dorsal and ventral sites, which may explain the opposing preference and aversion behaviors. However, we found that there was no significant difference in the number of dyn mRNA-expressing neurons between the dNAcSh and vNAcSh (Figure 5A– 5C, S5A, and S5B). This agreed with our anti-dyn staining where there was also no significant difference in dyn-labeled cells in the dorsal and ventral shell (Figure 5D). Both dorsal and ventral dyn mRNA+ neurons in the NAcSh also show increased colocalization (92%) with *Drd1*-containing neurons compared to *Drd2*-containing neurons (7%) (Figures 5A, 5B, 5D, S5A, and S5B). These data support the conclusion that colocalization of dyn with D1 receptors is not differentially segregated within these regions of the NAcSh and is therefore unlikely to be responsible for the opposing behaviors we observed.

Aversion and Preference Following Photostimulation of Dyn-Expressing Neurons in the NAcSh Requires KOR Activity

Current research indicates a role for NAc KORs in aversive negative affective behaviors involved in stress, dysphoria, and drug abuse (Bals-Kubik et al., 1989; Land et al., 2009; Mucha et al., 1985; Shippenberg et al., 2007; Solecki et al., 2009). Therefore, we hypothesized that activation of KORs following the photostimulated release of dyn in the ventral NAc is one of the key underlying mechanisms for the observed aversion behavior.

From this point onward we modified our viral injection volume and coordinates to specifically target either the dorsal or vNAcSh. We also injected AAV5-DIO-ChR2-eYFP into dyn-cre⁻ control mice in either the dorsal and ventral NAc and saw no effect of photostimulation in either group. Based on the results from our whole-cell slice recordings and in vivo frequency response data, we photostimulated at 10 Hz with a 10-ms pulse width to elicit action potential firing, remain physiologically relevant, and maintain reliable spike fidelity. We first assessed how photostimulation of dyn-expressing cells in the vNAcSh drives an aversion in a conditioned place-testing paradigm. This
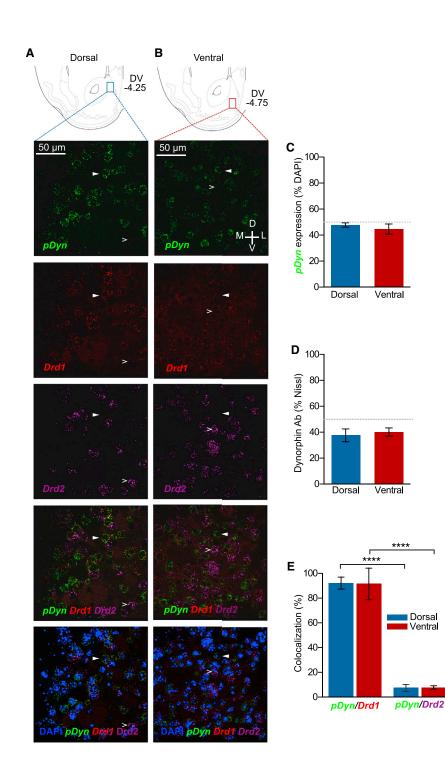
(A) Cartoon depicting the anatomical location of the dorsal (blue) subregion of the NAcSh corresponding to images as well as quantification. Representative 40× images of *pDyn* (green), *Drd1* (red), and *Drd2* (purple) mRNA expression in the dorsal shell.

(B) Cartoon depicting the anatomical location of the ventral (red) subregions of the NAcSh corresponding to microscope images as well as quantification. Representative 40× images of *pDyn* (green), *Drd1* (red), and *Drd2* (purple) mRNA expression in the ventral shell.

(C) No significant difference in dyn mRNA-expressing neurons between the dNAcSh and vNAcSh.

(D) No significant difference in anti-dyn antisera-positive cells in the dNAcSh or vNAcSh (data represented as mean ± SEM, n = 3).

(E) Dorsal and ventral NAcSh dyn mRNA⁺ neurons show increased colocalization with *Drd1*-containing neurons compared to *Drd2*-containing neurons. (Data represented as mean ± SEM, n = 5, ****p < .0001, one-way ANOVA, Bonferroni post hoc.)

tostimulation of dNAcSh was able to drive a significant preference behavior when compared to either controls or one another (Figures 6B and 6C).

To test the hypothesis that the aversion behavior is mediated by the release of dyn from cells within the vNAcSh acting on local KORs, we locally infused the long-acting KOR antagonist NorBNI (2.5 μg/1 μl) (Bruchas et al., 2007; Al-Hasani et al., 2013a; Melief et al., 2010) into the vNAcSh 14 days after site-specific AAV5-DIO-ChR2-eYFP injection in to the vNAcSh (Figure 6A). Importantly, injection of NorBNI into the vNAcSh was able to significantly block the aversion following photostimulation of dyn-expressing cells (Figures 6B, 6D, and 6E) with no observed change in locomotor activity (Figure S6C). A group of dyn-cre⁻ mice was injected with NorBNI as a control to ensure that NorBNI has no baseline effect on learning. These mice were statistically identical to the controls (Figures 6B, 6D, and 6E). These findings suggest that the aversion behavior mediated following photostimulation of dyn-expressing cells in the vNAcSh is in fact KOR mediated, acting locally within the NAc itself, consistent with prior studies using exogenous agonist and antagonist infusions within this region (Castro and Berridge, 2014; Land et al., 2009; Shippenberg et al., 2007). Interestingly, and somewhat unexpectedly, we also observed that NorBNI was able to block the preference behavior observed following photostimulation of

Pavlovian conditioning behavioral model is used to measure the motivational or aversive effects of an associated experience. The key component of this model is the learning aspect, which was absent in our RTPT paradigm (Figure 6A). We found that in a real-time Y-maze conditioning paradigm (Figure 6A) we are able to condition mice to the photostimulation of dyn-expressing cells in the vNAcSh to drive a learned aversion behavior, which is consistent with our earlier findings. In addition, conditioned pho-
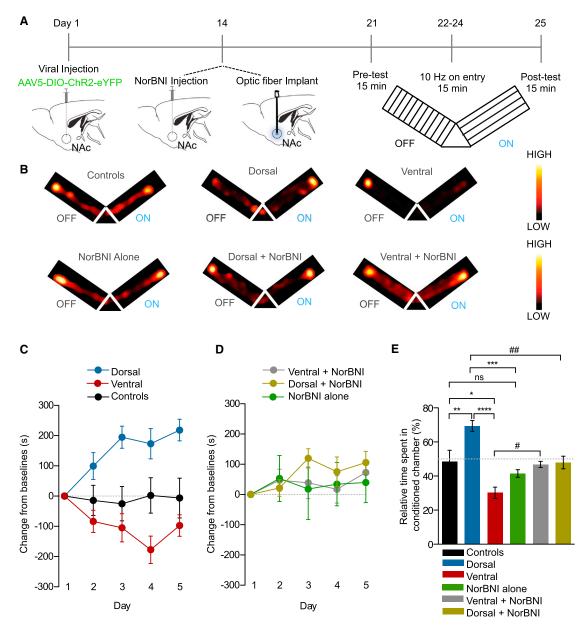
Figure 6. Preference and Aversion Following Photostimulation of Dyn-Containing Neurons in the Dorsal and vNAcSh Requires KOR Activity
(A) Calendar outlining the Y-maze paradigm.
(B) Representative activity heat maps from all groups during post-test.
(C) Change from baseline in dorsal, ventral, and control mice measured across all 5 days of the Y-maze paradigm (data represented as mean ± SEM, n = 8–13, two-way ANOVA, interaction effect between groups and days, p < 0.0001).
(D) Change from baseline in NorBNI+dorsal, NorBNI+ventral, and NorBNI alone mice measured across all 5 days of the Y-maze paradigm (data represented as mean ± SEM, n = 8–13).
(E) Change in percent time spent in conditioned arm of the Y-maze in all groups (data represented as mean ± SEM, n = 8–13; one-way ANOVA, Bonferroni post hoc, control versus dorsal **p < 0.01, Control versus ventral *p < 0.05, dorsal versus ventral ****p < 0.0001, control versus NorBNI alone ns, dorsal versus NorBNI ***p < 0.001, dorsal versus dorsal+NorBNI ##p < 0.01, ventral versus ventral NorBNI #p < 0.05).

dyn-expressing in the dNAcSh (Figures 6B, 6D, and 6E). This finding, while surprising, is supported by the recent findings of Castro and Berridge (2014), who show that agonist activation of KOR in discrete regions of the NAc can drive preference/appetitive behaviors.

Distinct NAc Dyn Populations in Operant Stimulation Produce Positive and Negative Responses

The operant self-stimulation paradigm uniquely demonstrates the ability of a mouse to establish response habits similar to those exhibited to natural reward. Here we assessed the
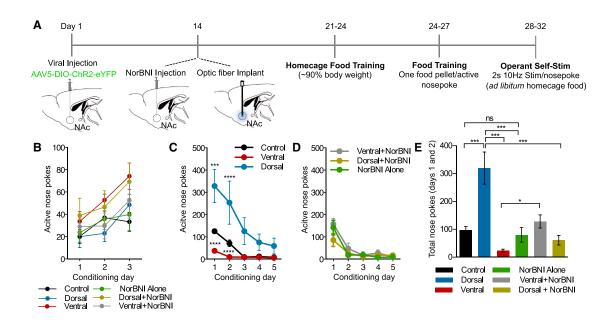
Figure 7. Distinct NAc Dyn Populations in Operant Stimulation Produce Positive and Negative Responses

(A) Calendar outlining the operant self-stimulation paradigm.

(B) No significant difference in active nose pokes for food reward between all groups (data represented as mean ± SEM, n = 6 to 7).

(C) Data showing number of nose pokes across 5 day of operant self-stimulation. Dorsally injected mice show significantly increased active nose pokes, compared to controls and ventrally injected mice, which show a significant reduction in nose pokes following photostimulation (data represented as mean ± SEM, n = 6 to 7: two way repeated-measures ANOVA, Bonferroni post hoc; dorsal versus controls on day 1 ***$p < 0.001$, dorsal versus controls on day 2 **$p < 0.001$, dorsal versus ventral on day 1 and 2 ****$p < 0.0001$.)

(D) Data showing number of nose pokes across 5 days of operant self-stimulation with no significant differences between ventral+NorBNI, dorsal+NorBNI, and NorBNI alone (data represented as mean ± SEM, n = 6 to 7).
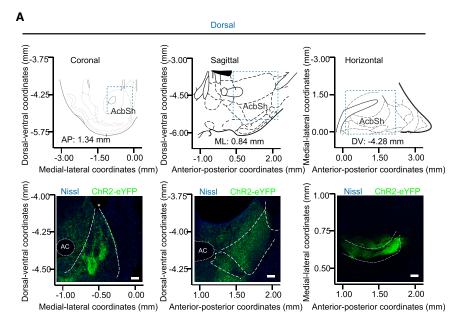
(E) Significant differences in total nose pokes on day 1 and day 2 following photostimulation (data represented as mean ± SEM, n = 6 to 7: one-way ANOVA, Bonferroni post hoc; control versus dorsal ***$p < 0.0001$, dorsal versus ventral ***$p < 0.0001$, ventral versus ventral+NorBNI *$p < 0.01$, dorsal versus dorsal+NorBNI, dorsal versus NorBNI alone ***$p < 0.001$, control versus NorBNI alone ns).
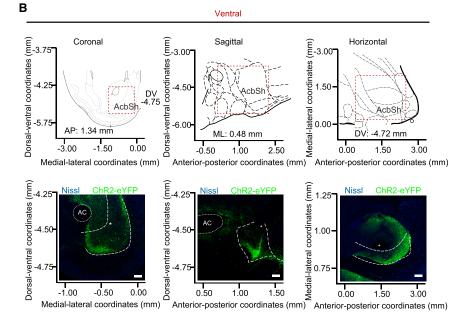
Representative 60-min trials for each group.

contribution of dNAcSh and vNAcSh dyn-expressing neurons in self-stimulation (Figure 7A). Importantly, all groups of mice were able to learn to nose poke at the same rate for a food reward (Figure 7B). Following food training, the food pellet was replaced with a 2-s (10 Hz, 10 ms pulse width) photostimulation, which was delivered following a nose poke. The dorsally injected mice continued to show positive reinforcement behavior, but the number of nose pokes increased 5-fold following photostimulation, emphasizing the highly rewarding nature of self-stimulation of this NAcSh subregion (Figures 7C, 7E, S7B, and S7E; Movie S1). However, both the controls and the ventrally injected mice decreased their number of nose pokes following photostimulation, which was significantly different compared to the dorsally injected mice (Figures 7C and 7E). The aversive nature of the photostimulation in the vNAcSh suggests that it is strong enough to mute the characteristic extinction burst seen during the first day of photostimulation and accelerate extinction following food training. Whereas the dorsally injected mice maintain an increased number of nose pokes due to the reinforcing nature of the photostimulation (Figures 7C, 7E, S7B, and S7E). Furthermore, NorBNI locally infused into these subregions blocked both the positive and negative behaviors displayed in this self-stimulation operant model (Figures 7D,

7E, S7C, and S7G–S7I). In addition, treatment of NorBNI alone was not significantly different from controls, suggesting that NorBNI infusion by itself within this structure does interfere with learning processes, consistent with prior reports (Land et al., 2008) (Figures 7D, 7E, S7C, and S7G). These operant self-stimulation data further suggest that there is a dynamic relationship between the positively reinforcing and aversive nature of stimulating distinct subpopulations of NAcSh Dyn-containing cells, both of which appear to be mediated by local KORs.

DISCUSSION

In the present study, we identify that photostimulation of dyn-expressing cells in discrete subregions within the NAcSh drive opposing motivational behavioral states. We show that photostimulation of dyn-expressing cells in the vNAcSh drives aversion behavior whereas photostimulation in the dNAcSh drives a preference/reward behavior. Here we demonstrate this functional anatomical segregation using three different behavioral paradigms; real-time place testing using bidirectional wireless μ-ILED technology, conditioned place testing, and operant self-stimulation.

A

Dorsal

Coronal
Dorsal-ventral coordinates (mm)
AcbSh
AP: 1.34 mm
Medial-lateral coordinates (mm)

Sagittal
Dorsal-ventral coordinates (mm)
AcbSh
ML: 0.84 mm
Anterior-posterior coordinates (mm)

Horizontal
Medial-lateral coordinates (mm)
AcbSh
DV: -4.28 mm
Anterior-posterior coordinates (mm)

Nissl ChR2-eYFP
Dorsal-ventral coordinates (mm)
AC
Medial-lateral coordinates (mm)

Nissl ChR2-eYFP
Dorsal-ventral coordinates (mm)
AC
Anterior-posterior coordinates (mm)

Nissl ChR2-eYFP
Medial-lateral coordinates (mm)
Anterior-posterior coordinates (mm)

B

Ventral

Coronal
Dorsal-ventral coordinates (mm)
AcbSh
DV -4.75
AP: 1.34 mm
Medial-lateral coordinates (mm)

Sagittal
Dorsal-ventral coordinates (mm)
AcbSh
ML: 0.48 mm
Anterior-posterior coordinates (mm)

Horizontal
Medial-lateral coordinates (mm)
AcbSh
DV: -4.72 mm
Anterior-posterior coordinates (mm)

Nissl ChR2-eYFP
Dorsal-ventral coordinates (mm)
AC
Medial-lateral coordinates (mm)

Nissl ChR2-eYFP
Dorsal-ventral coordinates (mm)
AC
Anterior-posterior coordinates (mm)

Nissl ChR2-eYFP
Medial-lateral coordinates (mm)
Anterior-posterior coordinates (mm)

Figure 8. Characterization of Viral Expression and Fiber Placement throughout the NAc

(A and B) Coronal, sagittal, and horizontal views documenting NAc dyn-dependent viral expression in dorsally injected mice (A) that demonstrated reward-like behaviors and ventrally injected mice (B) that demonstrated aversion behaviors. Top panels use stereotaxic coordinates and atlas images to orient the location of bottom panels of representative confocal micrographs. Scale bars, 100 μm. * indicates tissue damage from fiber placements.

traditionally mediates an increase in "liking" following mu opioid receptor (MOR) activation; however, a role has also been identified for both delta opioid receptors (DOR) and KOR (Castro and Berridge, 2014). Within this recent body of work, a separate suppressive cold spot in the caudal half of the shell was identified in which each opioid stimulation oppositely reduced sucrose positive "liking" reactions (Castro and Berridge, 2014). In addition to these findings, this group identified several anatomical differences between NAc opioid control of "liking" verses "wanting" of feeding (Castro and Berridge, 2014). These results not only highlight the anatomical heterogeneity of the NAc but also show that this is localized to opioid reward-related functions in the medial shell, which includes a role for the KOR system. While using a different species and behavioral model and focusing on the dorsal/ventral axis rather than the rostral/caudal axis, we report consistent endogenous dynorphinergic heterogeneity within the NAcSh. Here, selective photostimulation of the endogenous dyn-expressing cells in the dNAcSh drives a preference/reward behavior, but photostimulation of dyn-expressing neurons in the vNAcSh drives

Previous studies reported that the dyn/KOR system mediates negative emotional states likely through increased dyn release in the NAc, contributing to the dysphoria associated with depression, drug dependence, and withdrawal, but the mechanisms for engagement of dyn circuitry were unknown (Britton et al., 1982; Bruchas et al., 2009; Knoll et al., 2011; Lindholm et al., 2000; Mucha et al., 1985; Pfeiffer et al., 1986; Rylkova et al., 2009; Schlosburg et al., 2013; Shippenberg et al., 2007). In this study, we demonstrate that discrete activation of dyn-expressing cells within the vNAcSh drives an aversion behavior. It was shown that the rostrodorsal quadrant of the medial NAcSh in rats contains a specialized opioid hedonic hotspot, which

aversion behavior. Furthermore, a recent study has found that prodynorphin content specifically in the vNAcSh is dramatically increased following 12-hr-long access heroin self-administration, and that escalation of this drug-seeking behavior was suppressed following treatment with the long-acting KOR antagonist NorBNI (Schlosburg et al., 2013). These findings further support our data and suggest that dyn tone in distinct subregions within the NAcSh can drive opposing motivated behavioral states. We show the specific location of the virus and more importantly the fiber optic tip through all three coronal, sagittal, and horizontal planes to help identify the two distinct dorsal and ventral shell regions that drive these opposing behaviors (Figure 8).

To discretely isolate these small subregions of the NAc within a single animal, we modified our wireless, spatially targeted μ-ILED devices (Jeong et al., 2015; Kim et al., 2013; McCall et al., 2013) to enable independent illumination of either the ventral or dorsal region of the NAc within the same mouse. We generated this modified version to directly test the question of spatial segregation of reward and aversion within the NAcSh and were able to induce a real-time aversion and reward behavior within the same mouse to show that engaging dyn neurons in these discrete regions mediates opposing behaviors. Importantly, we also found that stimulating these distinct regions does not mediate an anxiety-like behavior, consistent with previous reports that identify the amygdala as the KOR site involved in anxiety-like behaviors (Bruchas et al., 2009; Knoll et al., 2011).

Looking closely at the neurobiological sources of dyn and KOR in the NAc, it is widely known that dyn is predominantly expressed in MSNs within the NAc that coexpress dopamine D1 receptors. However, there are also input projections from other structures that could release dyn, such as the ventral pallidum and the lateral hypothalamus (Baldo et al., 2003; Groenewegen et al., 1999; Haber et al., 1985; Peyron et al., 1998). KORs have been shown to have a somewhat heterogeneous cellular distribution within the NAcSh, in line with their role in the direct and indirect modulation of excitatory transmission (Svingos et al., 1999). It is reported that postsynaptic KORs in the NAc are on dendrites of most MSNs but reside predominantly on the dopamine-D2-expressing MSNs (Svingos et al., 1999). KORs are also widely known to be expressed on presynaptic terminals of glutamate, serotonin, and dopamine projections into the NAc (Bruchas et al., 2011; Hjelmstad and Fields, 2001; Land et al., 2009; Schindler et al., 2012; Svingos et al., 1999). In light of this, we hypothesized that the dyn-mediated aversion in the vNAcSh is driven by activation of KOR locally in the NAc. In both a conditioned place preference and an operant self-stimulation paradigm, we show that NorBNI is able to block the aversion behavior following photostimulation of dyn neurons in the vNAcSh, thereby identifying that aversion behavior in the vNAcSh is mediated by a local KOR-dependent mechanism.

Photostimulation of dyn-expressing cells in the dNAcSh also drives a preference/reward behavior in all three paradigms. This finding is intriguing in light of the widely accepted role of the dyn/KOR system in aversive/dysphoric behaviors. In addition to localizing in NAc GABAergic MSNs, dyn-expressing cells also express substance P (Lee et al., 1997; Napier et al., 1995) and synapse onto cholinergic neurons that express NK1 receptors (Martone et al., 1992; Pickel et al., 1976). The subsequent activation of these receptors is thought to be involved in cue signaling reward and learning (Elliott et al., 1986; Graybiel et al., 1994). Based on these findings, we thought perhaps the stimulation of dyn-expressing cells modulates substance P/cholinergic signaling to drive the observed preference behavior. However, subsequent experiments show that the positive rewarding effects appear to be mediated by KOR activation, as NorBNI is able to block these rewarding effects. Interestingly, the Berridge group is the first to report rewarding effects for kappa activation, but this was restricted to the rostrodorsal shell hotspot, as all other areas produced negative effects (Castro and Berridge, 2014). They suggest that the anatomical specificity gates the valence of KOR effects in the NAc, which in turn seems to be the case with our current findings. How KOR is able to mediate these opposing behaviors in two distinct regions of the NAcSh is unknown, but it is likely modulated by functionally distinct neuronal populations projecting to either the dorsal or ventral shell. This concept was well demonstrated in a recent study identifying distinct neuronal population projections from the BLA to the NAc code for positive valence, but projections to the central nucleus of the amygdala code for negative valence (Namburi et al., 2015). In addition, novel signaling within mesoaccumbens fibers in which both glutamate and dopamine can both be released from the same axons has recently been identified (Zhang et al., 2015). Furthermore, there is new evidence showing that projections from the NAc to the ventral pallidum do not conform to the traditionally accepted model of D1-direct and D2-indirect neuronal communication (Kupchik et al., 2015). Complex neuronal characteristics such as these in conjunction with the analysis of discrete projections may help us to dissect how the KOR in the NAcSh can mediate both a preference and aversion behavior via separable populations. Furthermore, the current findings we report here corroborate the elegant work of Thompson and Swanson (2010), which identified network nodes within the NAc that are localized and restricted to specific subdivisions within a region (Thompson and Swanson, 2010). Mapping the distinct projections to and from discrete regions in future studies with the dyn-reporter mouse (dyn-Cre^tdTomato) and viral tracing approaches will help us to understand what is driving the unique behavioral outputs in this present study and how these populations are engaged, altered, and recruited in stress- and reward-related behaviors.

Here we have identified two distinct subregions within the NAcSh that drive opposing behaviors through activation of the KOR/dyn system. Photostimulation of dyn-expressing neurons in the vNAcSh causes a KOR-dependent aversive behavior, whereas photostimulation of dyn-expressing neurons in the dNAcSh causes preference. Understanding the circuitry that mediates motivated behaviors is critical in furthering our understanding of positive and negative affective states that contribute to mood disorders, addiction, and depression.

EXPERIMENTAL PROCEDURES

Additional detailed methods provided in the Supplemental Experimental Procedures.

Experimental Subjects and Stereotaxic Surgery

Adult (25–35 g) male preprodynorphin-IRES-cre (dyn-Cre) mice were group-housed, given access to food pellets and water ad libitum, and maintained on a 12 hr:12 hr light:dark cycle (lights on at 7:00 AM). All animals were kept in a sound-attenuated, isolated holding facility in the lab 1 week prior to surgery, post-surgery, and throughout the duration of the behavioral assays to minimize stress. All procedures were approved by the Animal Care and Use Committee of Washington University and conformed to US National Institutes of Health guidelines. For surgery, mice were anesthetized in an induction chamber (4% Isoflurane) and placed into a stereotaxic frame (Kopf Instruments, Model 1900) where they were maintained at 1%–2% isoflurane. We performed a craniotomy and unilaterally injected, using a blunt needle (86200, Hamilton Company), 300 nl of AAV5-DIO-ChR2-eYFP or AAV5-DIO-eYFP (Hope Center Viral Vector Core, viral titer 2 × 10^13 vg/ml) into either the dNAcSh (stereotaxic coordinates from bregma: +1.30 anterior-posterior

[AP], ±0.5 medial-lateral [ML], −4.25 mm dorsal-ventral [DV]) or vNAcSh (stereotaxic coordinates from bregma: +1.30 [AP], ±0.5 [ML], −4.75 mm [DV]), followed by fiber optic implantation (Sparta et al., 2012). We secured the implants using two bone screws and a dental dental cement headcap (Lang Dental). Mice were allowed to recover for 3 weeks prior to behavioral testing, permitting optimal expression of ChR2 in the Dyn-Cre cell bodies. For NorBNI local Infusion, mice were locally injected with NorBNI in the vNAcSh (2.5 μg/1 μl) and implanted with a fiber optic 2 weeks prior to behavior. These mice were allowed at least 1 week to recover post-surgery before beginning experimentation, well within the limits of norBNI antagonism.

Generation and Breeding of Pdyn-IRES-cre Mice and Ai9-x Pdyn-IRES-cre

Pdyn-IRES-cre mice were kindly provided by Bradford Lowell's lab (Krashes et al., 2014). The mice were bred at Washington University in Saint Louis by crossing the pdyn-IRES-cre mice with C57BL/6 wild-type mice and back-crossed for seven generations. These mice were then crossed to Ai9-tdTomato mice on C57BL/6 background, bred, and backcrossed for seven generations.

Immunohistochemistry and Quantification

Immunohistochemistry and quantification was performed as previously described (Al-Hasani et al., 2013b; Kim et al., 2013; McCall et al., 2015). To ensure no bleed through from the bright tdTomato signaling, a very conservative bandwidth was used to collect the Alexa 488 signal (498–520 nm), and a red shifted bandwidth was used for the tdTomato signal (600–700 nm). These were also compared to a negative control (no 1° Ab).

Slice Electrophysiology

We performed whole-cell electrophysiology experiments similar to those published (Sparrow et al., 2012). Briefly, mice were rapidly decapitated under isoflurane anesthesia, and 300 μM coronal slices containing the NAc were prepared on a vibratome (Leica VT1200). The brains were removed and placed in ice-cold modified high sucrose artificial cerebrospinal fluid (aCSF). Slices were then transferred to normal aCSF maintained at ∼30° (Warner Instruments). Slices were placed in a holding chamber (Warner Instruments) and were allowed to rest for 1 hr. Slices were continuously bubbled with a 95% O_2/5% CO_2 mixture throughout slicing and experiments. Patch pipettes (3–6 MΩ) were pulled from thin-walled borosilicate glass on a Flaming-Brown Micropipette Puller (Sutter Instruments). Following rupture of the cell membrane, cells were allowed to rest and equilibrate to the intracellular recording solutions. Input resistance was monitored continuously throughout the experiment, and when input resistance deviated by more than 20%, the experiment was discarded. Light-evoked action potentials in the NAc were recorded using a potassium-gluconate-based internal. Action potentials were light-evoked at frequencies from 5 to 40 Hz to determine spike fidelity. Light-evoked IPSC recordings exclusively from non-dynorphin neurons in the vNAcSh were conducted in voltage clamp using a cesium-methansulfonate-based internal solution so that we could detect EPSCs (−55 mV) and IPSCs (+10 mV) in the same neuron. After confirming the absence of light-evoked EPSC signal, we measured light-evoked IPSCs during a single 10-ms light pulse of 470 nm. In a subset of these experiments, SR95531 (GABAzine, 10 μM) was bath applied for 10 min to block IPSCs. All solutions can be found in the Supplemental Experimental Procedures.

Peptide Enzyme Immunoassay to Measure Photostimulated Release of Dyn

3 weeks post-viral injection, mice were intracardially perfused with aCSF, and 150 μm sections were taken using a vibrotome (Leica). Slices containing the NAc were allowed to acclimate at 30°C in aerated NMDG aCSF for 10 min before being transferred to recovery aCSF at room temperature for 20 to 40 min. Slices from each animal were collected in a glass vial containing 500 μl of recovery aCSF. A 473-nm laser (10 Hz, 10 ms pulse width) was directed to the bottom of the glass vial containing the slices for 15 min. Following photostimulation, 8 × 50 μl of the recovery aCSF from within the vial was pipetted into a 96-well plate as per Peninsula Protocol II (Peninsula Labs). Absorbance was measured at 650 nm using a SynergyMx microplate reader (BioTek). Dyn release was quantified in ng/ml and compared to dyn-cre⁻ controls.

Behavior

All behaviors were performed within a sound-attenuated room maintained at 23°C at least 1 week after habituation to the holding room and the final surgery. Lighting was stabilized at ∼1,500 lux for aversion behaviors, ∼250 lux for anxiety-like behaviors. Movements were video recorded and analyzed using Ethovision XT 8.5 (Noldus Information Technologies). At the end of each study, animals were perfused with 4% paraformaldehyde followed by anatomical analysis to confirm injection sites and cell-type-specific expression.

Real-Time Place Testing

Mice were placed in a custom-made unbiased, balanced two-compartment conditioning apparatus (52.5 × 25.5 × 25.5 cm) as described previously (McCall et al., 2015; Siuda et al., 2015b). During a 20-min trial, entry into one compartment triggered photostimulation of various frequencies (5, 10, 20, 40 Hz, etc.) while the animal remained in the light-paired chamber and entry into the other chamber ended photostimulation.

Y-Maze Conditioned Place Testing

Mice were placed in a three-chambered environment compatible with fiber optics coupled to 473-nm laser as previously described (Kim et al., 2013). On day 1 (pre-test), the mice have free access to all chambers without stimulation to show no bias between the two larger, cue-distinct environments. This is followed by three conditioning days where upon entry into one chamber photostimulation (10 Hz, 10 ms pulse width) occurs in real-time, and when the animal leaves this compartment photostimulation ends. On day 5 (post-test), mice have free access to all chambers without stimulation to assess whether a preference or aversion association has been made with the paired context. Data were calculated as time spent in each chamber and entries into the photostimulation-paired chamber.

Operant Self-Stimulation

Mice are initially food deprived to 90% of their body weight and trained to nose poke for food pellets for 4 days in a modular test chamber for mice (17.8 cm × 15.2 cm × 18.4 cm) (Med Associates Inc.). This was used in conjunction with either Ethovision XT (Noldus) or MED-PC (Med Associates Inc.). This was followed by operant self-stimulation where upon an active nose poke the mice receive a 2-s photostimulation (10 Hz, 10 ms pulse width stimulation) on a fixed ratio-1 schedule for a 1 hr session. For operant self-stimulation, the mice are connected to a laser via a tether that runs through the top of the chamber. An Arduino (http://www.arduino.cc/) is programed and connected to the laser and chamber so upon nose poking the 2 s, 10 Hz, 10-ms pulse width photostimulation is administered paired with a cue light and a tone. An inactive nose poke resulted in no stimulation, cue light, or tone. The data were calculated as total number of nose pokes at the active and inactive for each day over the course of 5 days.

Wireless Powering and RF Powering Scavenger

Wireless powering of the μ-ILED devices was adapted as previously described (Kim et al., 2013; McCall et al., 2013). The RF scavenger consists of antennas, impedance matching circuits, and Cockcroft-Walton voltage multiplier. The wireless power transmitter includes an RF signal generator (Agilent N5181A), a power supply (Agilent U8031A), a RF power amplifier (Empower RF Systems 1119-BBM3K5KHM), an RF signal splitter (RF Lambda RFLT2W0727GN), and two panel antennas (ARC Wireless ARC-PA2419B01). The RF signal generator is internally modulated to deliver sufficient power to light the μ-ILEDs at the given stimulation protocol (10 Hz, 50 ms pulse widths). The modulated RF signal is amplified and transmitted from the panel antenna to the headstage power harvesters. The RF signal generator has a power output from −10 to 0 dBm at 1.5 GHz and 2.4 GHz for each LEDs, optimized daily to ensure equivalent light power in the assay. Mice with chronically implanted μ-ILED devices were acutely connected to the headstage power harvesters immediately prior to any wireless photostimulation.

RNAscope Fluorescent In Situ Hybridization

Following rapid decapitation of C57/BL6 mice, brains were rapidly frozen in 100 ml −50°C isopentane and stored at −80°C. Coronal sections containing the NAc, corresponding to the injection plane used in the behavioral

experiments, were cut at 20 μM at −20°C and thaw-mounted onto Super Frost Plus slides (Fisher). Slides were stored at −80°C until further processing. Fluorescent in situ hybridization was performed according to the *RNAScope 2.0 Fluorescent Multiple Kit User Manual for Fresh Frozen Tissue* (Advanced Cell Diagnostics, Inc.) as described by Wang et al. (2012). Briefly, sections were fixed in 4% PFA, dehydrated, and treated with *pretreatment 4* protease solution. Sections were then incubated for target probes for mouse prodynorphin (*pDyn*-C1, accession number NM_018863.3, probe region 33–700) dopamine receptor 1 (*Drd1*-C2, accession number NM_010076.3, probe region 463–1,336), and dopamine receptor 2 (*Drd2*-C3, accession number NM_010077.2, 85–1,153). All target probes consisted of 20 ZZ oligonucleotides and were obtained from Advanced Cell Diagnostics. Following probe hybridization, sections underwent a series of probe signal amplification steps followed by incubation of fluorescently labeled probes designed to target the specified channel associated with *pDyn* (C1 – Alexa 488), *Drd1* (C2 – Atto 550), and *Drd2* (C3 – Atto 647). Slides were counterstained with DAPI, and coverslips were mounted with Vectashield Hard Set mounting medium (Vector Laboratories). Images were obtained on a Leica TCS SPE confocal microscope and analyzed with Application Suite Advanced Fluorescence (Leica).

Statistics

All data are expressed as mean ± SEM. Statistical significance was taken as *$p < 0.05$, **$p < 0.01$, ***$p < 0.001$, and ****$p < 0.0001$, as determined by a one-way ANOVA or a two-way repeated-measures ANOVA followed by a Bonferroni post hoc tests as appropriate. Statistical analyses were performed in GraphPad Prism 5.0.

SUPPLEMENTAL INFORMATION

Supplemental Information includes seven figures and Supplemental Experimental Procedures and can be found with this article online at http://dx.doi.org/10.1016/j.neuron.2015.08.019.

AUTHOR CONTRIBUTIONS

Conceptualization, R.A.-H., J.G.M., and M.R.B.; Methodology, R.A.-H., J.G.M., A.M.G., G.S., C.-O.P., S.I.P., C.M.M., N.A.C., T.L.K., J.A.R., and M.R.B.; Investigation, R.A.-H., J.G.M., A.M.G, G.S., J.M.B., G.S., C.-O.P., S.I.P, C.M.M., and N.A.C.; Resources, M.J.K. and B.B.L.; Writing – Original Draft, Review & Editing, R.A.-H., J.G.M., and M.R.B.; Funding acquisition, M.R.B., R.A.-H.; Supervision, T.L.K., J.A.R.; Project administration, M.R.B.

ACKNOWLEDGMENTS

REFERENCES

Al-Hasani, R., McCall, J.G., Foshage, A.M., and Bruchas, M.R. (2013a). Locus coeruleus kappa opioid receptors modulate reinstatement of cocaine place preference through a noradrenergic mechanism. Neuropsychopharmacology *38*, 2484–2497.

Al-Hasani, R., McCall, J.G., Foshage, A.M., and Bruchas, M.R. (2013b). Locus coeruleus kappa-opioid receptors modulate reinstatement of cocaine place preference through a noradrenergic mechanism. Neuropsychopharmacology *38*, 2484–2497.

Baldo, B.A., Daniel, R.A., Berridge, C.W., and Kelley, A.E. (2003). Overlapping distributions of orexin/hypocretin- and dopamine-beta-hydroxylase immunoreactive fibers in rat brain regions mediating arousal, motivation, and stress. J. Comp. Neurol. *464*, 220–237.

Bals-Kubik, R., Herz, A., and Shippenberg, T.S. (1989). Evidence that the aversive effects of opioid antagonists and kappa-agonists are centrally mediated. Psychopharmacology (Berl.) *98*, 203–206.

Britt, J.P., Benalioued, F., McDevitt, R.A., Stuber, G.D., Wise, R.A., and Bonci, A. (2012). Synaptic and behavioral profile of multiple glutamatergic inputs to the nucleus accumbens. Neuron *76*, 790–803.

Britton, D.R., Koob, G.F., Rivier, J., and Vale, W. (1982). Intraventricular corticotropin-releasing factor enhances behavioral effects of novelty. Life Sci. *31*, 363–367.

Bruchas, M.R., Land, B.B., Aita, M., Xu, M., Barot, S.K., Li, S., and Chavkin, C. (2007). Stress-induced p38 mitogen-activated protein kinase activation mediates kappa-opioid-dependent dysphoria. J. Neurosci. *27*, 11614–11623.

Bruchas, M.R., Land, B.B., Lemos, J.C., and Chavkin, C. (2009). CRF1-R activation of the dynorphin/kappa opioid system in the mouse basolateral amygdala mediates anxiety-like behavior. PLoS ONE *4*, e8528.

Bruchas, M.R., Land, B.B., and Chavkin, C. (2010). The dynorphin/kappa opioid system as a modulator of stress-induced and pro-addictive behaviors. Brain Res. *1314*, 44–55.

Bruchas, M.R., Schindler, A.G., Shankar, H., Messinger, D.I., Miyatake, M., Land, B.B., Lemos, J.C., Hagan, C.E., Neumaier, J.F., Quintana, A., et al. (2011). Selective p38α MAPK deletion in serotonergic neurons produces stress resilience in models of depression and addiction. Neuron *71*, 498–511.

Carter, M.E., Yizhar, O., Chikahisa, S., Nguyen, H., Adamantidis, A., Nishino, S., Deisseroth, K., and de Lecea, L. (2010). Tuning arousal with optogenetic modulation of locus coeruleus neurons. Nat. Neurosci. *13*, 1526–1533.

Castro, D.C., and Berridge, K.C. (2014). Opioid hedonic hotspot in nucleus accumbens shell: mu, delta, and kappa maps for enhancement of sweetness "liking" and "wanting". J. Neurosci. *34*, 4239–4250.

Chavkin, C., James, I.F., and Goldstein, A. (1982). Dynorphin is a specific endogenous ligand of the kappa opioid receptor. Science *215*, 413–415.

Daunais, J.B., Roberts, D.C., and McGinty, J.F. (1993). Cocaine self-administration increases preprodynorphin, but not c-fos, mRNA in rat striatum. Neuroreport *4*, 543–546.

Drevets, W.C., Videen, T.O., Price, J.L., Preskorn, S.H., Carmichael, S.T., and Raichle, M.E. (1992). A functional anatomical study of unipolar depression. J. Neurosci. *12*, 3628–3641.

Elliott, P.J., Nemeroff, C.B., and Kilts, C.D. (1986). Evidence for a tonic facilitatory influence of substance P on dopamine release in the nucleus accumbens. Brain Res. *385*, 379–382.

Everitt, B.J., and Robbins, T.W. (2005). Neural systems of reinforcement for drug addiction: from actions to habits to compulsion. Nat. Neurosci. *8*, 1481–1489.

Fagergren, P., Smith, H.R., Daunais, J.B., Nader, M.A., Porrino, L.J., and Hurd, Y.L. (2003). Temporal upregulation of prodynorphin mRNA in the primate striatum after cocaine self-administration. Eur. J. Neurosci. *17*, 2212–2218.

Ghazarossian, V.E., Chavkin, C., and Goldstein, A. (1980). A specific radioimmunoassay for the novel opioid peptide dynorphin. Life Sci. *27*, 75–86.

Graybiel, A.M., Aosaki, T., Flaherty, A.W., and Kimura, M. (1994). The basal ganglia and adaptive motor control. Science *265*, 1826–1831.

Groenewegen, H.J., Wright, C.I., Beijer, A.V., and Voorn, P. (1999). Convergence and segregation of ventral striatal inputs and outputs. Ann. N Y Acad. Sci. *877*, 49–63.

Haber, S.N., Groenewegen, H.J., Grove, E.A., and Nauta, W.J. (1985). Efferent connections of the ventral pallidum: evidence of a dual striato pallidofugal pathway. J. Comp. Neurol. 235, 322–335.

Hjelmstad, G.O., and Fields, H.L. (2001). Kappa opioid receptor inhibition of glutamatergic transmission in the nucleus accumbens shell. J. Neurophysiol. 85, 1153–1158.

Hurd, Y.L., Brown, E.E., Finlay, J.M., Fibiger, H.C., and Gerfen, C.R. (1992). Cocaine self-administration differentially alters mRNA expression of striatal peptides. Brain Res. Mol. Brain Res. 13, 165–170.

Jeong, J.-W., McCall, J.G., Shin, G., Zhang, Y., Al-Hasani, R., Kim, M., Li, S., Sim, J.Y., Jang, K.-I., Shi, Y., et al. (2015). Wireless Optofluidic Systems for Programmable In Vivo Pharmacology and Optogenetics. Cell 162, 662–674.

Kim, T.I., McCall, J.G., Jung, Y.H., Huang, X., Siuda, E.R., Li, Y., Song, J., Song, Y.M., Pao, H.A., Kim, R.-H., et al. (2013). Injectable, cellular-scale opto-electronics with applications for wireless optogenetics. Science 340, 211–216.

Knoll, A.T., Muschamp, J.W., Sillivan, S.E., Ferguson, D., Dietz, D.M., Meloni, E.G., Carroll, F.I., Nestler, E.J., Konradi, C., and Carlezon, W.A., Jr. (2011). Kappa opioid receptor signaling in the basolateral amygdala regulates conditioned fear and anxiety in rats. Biol. Psychiatry 70, 425–433.

Krashes, M.J., Shah, B.P., Madara, J.C., Olson, D.P., Strochlic, D.E., Garfield, A.S., Vong, L., Pei, H., Watabe-Uchida, M., Uchida, N., et al. (2014). An excitatory paraventricular nucleus to AgRP neuron circuit that drives hunger. Nature 507, 238–242.

Kravitz, A.V., Tye, L.D., and Kreitzer, A.C. (2012). Distinct roles for direct and indirect pathway striatal neurons in reinforcement. Nat. Neurosci. 15, 816–818.

Kupchik, Y.M., Brown, R.M., Heinsbroek, J.A., Lobo, M.K., Schwartz, D.J., and Kalivas, P.W. (2015). Coding the direct/indirect pathways by D1 and D2 receptors is not valid for accumbens projections. Nat. Neurosci. Published online July 27, 2015. http://dx.doi.org/10.1038/nn.4068.

Land, B.B., Bruchas, M.R., Lemos, J.C., Xu, M., Melief, E.J., and Chavkin, C. (2008). The dysphoric component of stress is encoded by activation of the dynorphin kappa-opioid system. J. Neurosci. 28, 407–414.

Land, B.B., Bruchas, M.R., Schattauer, S., Giardino, W.J., Aita, M., Messinger, D., Hnasko, T.S., Palmiter, R.D., and Chavkin, C. (2009). Activation of the kappa opioid receptor in the dorsal raphe nucleus mediates the aversive effects of stress and reinstates drug seeking. Proc. Natl. Acad. Sci. USA 106, 19168–19173.

Lee, T., Kaneko, T., Shigemoto, R., Nomura, S., and Mizuno, N. (1997). Collateral projections from striatonigral neurons to substance P receptor-expressing intrinsic neurons in the striatum of the rat. J. Comp. Neurol. 388, 250–264.

Lindholm, S., Ploj, K., Franck, J., and Nylander, I. (2000). Repeated ethanol administration induces short- and long-term changes in enkephalin and dynorphin tissue concentrations in rat brain. Alcohol 22, 165–171.

Madisen, L., Zwingman, T.A., Sunkin, S.M., Oh, S.W., Zariwala, H.A., Gu, H., Ng, L.L., Palmiter, R.D., Hawrylycz, M.J., Jones, A.R., et al. (2010). A robust and high-throughput Cre reporting and characterization system for the whole mouse brain. Nat. Neurosci. 13, 133–140.

Martone, M.E., Armstrong, D.M., Young, S.J., and Groves, P.M. (1992). Ultrastructural examination of enkephalin and substance P input to cholinergic neurons within the rat neostriatum. Brain Res. 594, 253–262.

Mayberg, H.S., Brannan, S.K., Tekell, J.L., Silva, J.A., Mahurin, R.K., McGinnis, S., and Jerabek, P.A. (2000). Regional metabolic effects of fluoxetine in major depression: serial changes and relationship to clinical response. Biol. Psychiatry 48, 830–843.

McCall, J.G., Kim, T.I., Shin, G., Huang, X., Jung, Y.H., Al-Hasani, R., Omenetto, F.G., Bruchas, M.R., and Rogers, J.A. (2013). Fabrication and application of flexible, multimodal light-emitting devices for wireless optogenetics. Nat. Protoc. 8, 2413–2428.

McCall, J.G., Al-Hasani, R., Siuda, E.R., Hong, D.Y., Norris, A.J., Ford, C.P., and Bruchas, M.R. (2015). CRH Engagement of the Locus Coeruleus Noradrenergic System Mediates Stress-Induced Anxiety. Neuron 87, 605–620.

Melief, E.J., Miyatake, M., Bruchas, M.R., and Chavkin, C. (2010). Ligand-directed c-Jun N-terminal kinase activation disrupts opioid receptor signaling. Proc. Natl. Acad. Sci. USA 107, 11608–11613.

Mucha, R.F., Millan, M.J., and Herz, A. (1985). Aversive properties of naloxone in non-dependent (naive) rats may involve blockade of central beta-endorphin. Psychopharmacology (Berl.) 86, 281–285.

Namburi, P., Beyeler, A., Yorozu, S., Calhoon, G.G., Halbert, S.A., Wichmann, R., Holden, S.S., Mertens, K.L., Anahtar, M., Felix-Ortiz, A.C., et al. (2015). A circuit mechanism for differentiating positive and negative associations. Nature 520, 675–678.

Napier, T.C., Mitrovic, I., Churchill, L., Klitenick, M.A., Lu, X.Y., and Kalivas, P.W. (1995). Substance P in the ventral pallidum: projection from the ventral striatum, and electrophysiological and behavioral consequences of pallidal substance P. Neuroscience 69, 59–70.

Peyron, C., Tighe, D.K., van den Pol, A.N., de Lecea, L., Heller, H.C., Sutcliffe, J.G., and Kilduff, T.S. (1998). Neurons containing hypocretin (orexin) project to multiple neuronal systems. J. Neurosci. 18, 9996–10015.

Pfeiffer, A., Brantl, V., Herz, A., and Emrich, H.M. (1986). Psychotomimesis mediated by kappa opiate receptors. Science 233, 774–776.

Pickel, V.M., Joh, T.H., and Reis, D.J. (1976). Monoamine-synthesizing enzymes in central dopaminergic, noradrenergic and serotonergic neurons. Immunocytochemical localization by light and electron microscopy. J. Histochem. Cytochem. 24, 792–306.

Raynor, K., Kong, H., Chen, Y., Yasuda, K., Yu, L., Bell, G.I., and Reisine, T. (1994). Pharmacological characterization of the cloned kappa-, delta-, and mu-opioid receptors. Mol. Pharmacol. 45, 330–334.

Russo, S.J., and Nestler, E.J. (2013). The brain reward circuitry in mood disorders. Nat. Rev. Neurosci. 14, 609–625.

Rylkova, D., Shah, H.P., Small, E., and Bruijnzeel, A.W. (2009). Deficit in brain reward function and acute and protracted anxiety-like behavior after discontinuation of a chronic alcohol liquid diet in rats. Psychopharmacology (Berl.) 203, 629–640.

Schindler, A.G., Messinger, D.I., Smith, J.S., Shankar, H., Gustin, R.M., Schattauer, S.S., Lemos, J.C., Chavkin, N.W., Hagan, C.E., Neumaier, J.F., and Chavkin, C. (2012). Stress produces aversion and potentiates cocaine reward by releasing endogenous dynorphins in the ventral striatum to locally stimulate serotonin reuptake. J. Neurosci. 32, 17582–17596.

Schlosburg, J.E., Whitfield, T.W., Jr., Park, P.E., Crawford, E.F., George, O., Vendruscolo, L.F., and Koob, G.F. (2013). Long-term antagonism of κ opioid receptors prevents escalation of and increased motivation for heroin intake. J. Neurosci. 33, 19384–19392.

Schlussman, S.D., Zhou, Y., Bailey, A., Ho, A., and Kreek, M.J. (2005). Steady-dose and escalating-dose "binge" administration of cocaine alter expression of behavioral stereotypy and striatal preprodynorphin mRNA levels in rats. Brain Res. Bull. 67, 169–175.

Shippenberg, T.S., Zapata, A., and Chefer, V.I. (2007). Dynorphin and the pathophysiology of drug addiction. Pharmacol. Ther. 116, 306–321.

Shirayama, Y., Ishida, H., Iwata, M., Hazama, G.-I., Kawahara, R., and Duman, R.S. (2004). Stress increases dynorphin immunoreactivity in limbic brain regions and dynorphin antagonism produces antidepressant-like effects. J. Neurochem. 90, 1258–1268.

Siuda, E.R., Copits, B.A., Schmidt, M.J., Baird, M.A., Al-Hasani, R., Planer, W.J., Funderburk, S.C., McCall, J.G., Gereau, R.W., 4th, and Bruchas, M.R. (2015a). Spatiotemporal control of opioid signaling and behavior. Neuron 86, 923–935.

Siuda, E.R., Copits, B.A., Schmidt, M.J., Baird, M.A., Al-Hasani, R., Planer, W.J., Funderburk, S.C., McCall, J.G., Gereau, R.W., 4th, and Bruchas, M.R. (2015b). Spatiotemporal control of opioid signaling and behavior. Neuron 86, 923–935.

Solecki, W., Turek, A., Kubik, J., and Przewlocki, R. (2009). Motivational effects of opiates in conditioned place preference and aversion paradigm–a study in three inbred strains of mice. Psychopharmacology (Berl.) 207, 245–255.

Sparrow, A.M., Lowery-Gionta, E.G., Pleil, K.E., Li, C., Sprow, G.M., Cox, B.R., Rinker, J.A., Jijon, A.M., Peña, J., Navarro, M., et al. (2012). Central neuropeptide Y modulates binge-like ethanol drinking in C57BL/6J mice via Y1 and Y2 receptors. Neuropsychopharmacology 37, 1409–1421.

Sparta, D.R., Stamatakis, A.M., Phillips, J.L., Hovelsø, N., van Zessen, R., and Stuber, G.D. (2012). Construction of implantable optical fibers for long-term optogenetic manipulation of neural circuits. Nat. Protoc. 7, 12–23.

Stamatakis, A.M., and Stuber, G.D. (2012). Activation of lateral habenula inputs to the ventral midbrain promotes behavioral avoidance. Nat. Neurosci. 15, 1105–1107.

Svingos, A.L., Colago, E.E., and Pickel, V.M. (1999). Cellular sites for dynorphin activation of kappa-opioid receptors in the rat nucleus accumbens shell. J. Neurosci. 19, 1804–1813.

Tan, K.R., Yvon, C., Turiault, M., Mirzabekov, J.J., Doehner, J., Labouèbe, G., Deisseroth, K., Tye, K.M., and Lüscher, C. (2012). GABA neurons of the VTA drive conditioned place aversion. Neuron 73, 1173–1183.

Thompson, R.H., and Swanson, L.W. (2010). Hypothesis-driven structural connectivity analysis supports network over hierarchical model of brain architecture. Proc. Natl. Acad. Sci. USA 107, 15235–15239.

Van Bockstaele, E.J., Gracy, K.N., and Pickel, V.M. (1995). Dynorphin-immunoreactive neurons in the rat nucleus accumbens: ultrastructure and synaptic input from terminals containing substance P and/or dynorphin. J. Comp. Neurol. 351, 117–133.

Wang, F., Flanagan, J., Su, N., Wang, L.-C., Bui, S., Nielson, A., Wu, X., Vo, H.-T., Ma, X.-J., and Luo, Y. (2012). RNAscope: a novel in situ RNA analysis platform for formalin-fixed, paraffin-embedded tissues. J. Mol. Diagn. 14, 22–29.

Zhang, S., Qi, J., Li, X., Wang, H.-L., Britt, J.P., Hoffman, A.F., Bonci, A., Lupica, C.R., and Morales, M. (2015). Dopaminergic and glutamatergic microdomains in a subset of rodent mesoaccumbens axons. Nat. Neurosci. 18, 386–392.